Liquid Metal Actuator for Inducing Chaotic Advection

Shi-Yang Tang, Vijay Sivan, Phred Petersen, Wei Zhang, Paul D. Morrison, Kourosh Kalantar-zadeh,* Arnan Mitchell,* and Khashayar Khoshmanesh**

Chaotic advection plays an important role in microplatforms for a variety of applications. Currently used mechanisms for inducing chaotic advection in small scale, however, are limited by their complicated fabrication processes and relatively high power consumption. Here, a soft actuator is reported which utilizes a droplet of Galinstan liquid metal to induce harmonic Marangoni flow at the surface of liquid metal when activated by a sinusoidal signal. This liquid metal actuator has no rigid parts and employs continuous electrowetting effect to induce chaotic advection with exceptionally low power consumption. The theory behind the operation of this actuator is developed and validated via a series of experiments. The presented actuator can be readily integrated into other microfluidic components for a wide range of applications.

1. Introduction

Chaotic advection in liquid can significantly improve the chemical reaction,[1,2] heat transfer,[3,4] chemical and biological transport[5,6] and mixing rate in microscale.[7–9] Methods for inducing chaotic advection in microfluidic systems can be classified in terms of the driving mechanism as: mechanical, thermal or electrical. Mechanically, the most straightforward way to produce chaotic advection in a microchannel is to induce secondary flows by patterning grooves or mechanical barriers along the flow,[7,10,11] or by utilizing curved geometries or multi-layer 3D structures.[12–14] However, fabrication process of such multi-layer structures is complicated, increasing the cost of the system.[15] Alternatively, surface acoustic waves (SAWs) generated by integrated piezoelectric ceramic transducers can be introduced into the liquid to drive chaotic advection.[16,17] However, it needs a relatively large voltage (>50 V) and high frequency (>10 MHz) with a power of >1 W to activate the transducer, which can induce unwanted heating and evaporation of the liquid.[17,18]

Thermally, local heating of the liquid by patterned microelectrodes or pointing a laser beam can cause chaotic advection due to natural convection mechanisms.[19–21] Electrically, schemes based on AC and DC electrokinetics, including dielectrophoresis,[22] electro-osmosis,[23–25] electro-hydrodynamics,[26,27] and electrowetting-on-dielectric[28] have been reported for producing chaotic advection for mixing applications. However, producing electrokinetic instability has several disadvantages, such as requiring a high operating voltage (in the kV range), strongly inhomogeneous electrical conductivity in the medium and high power supply, which is not accessible for conventional laboratories.[29] Additionally, the conductivity of the working liquid is limited due to bubble generation when a high DC voltage is applied.[26,29]

Therefore, a system that possesses features of rapid and efficient generation of chaotic advection, compact in size, easy to operate and maintain, low power consumption and can be readily integrated to other components can benefit many present-day and emerging applications in microfluidics.

Eutectic alloy base liquid metals, such as EGaIn (75% gallium and 25% indium)[30] and Galinstan (68.5% gallium, 21.5% indium and 10% tin)[31] offer remarkable properties including high electrical conductivity, high density, high surface tension, extremely low vapor pressure, and low toxicity in comparison to mercury.[31] These properties make them attractive for the development of microfluidic devices,[32] stretchable or makeshift components,[33–35] soft electronics,[30,36] MEMS devices,[37] and nanotechnology enabled applications.[38–41] We have recently developed a small scale pumping system called "Liquid Metal Enabled Pump", in which a droplet of Galinstan serves as the core of the pump with no conventional mechanical moving parts for pumping liquid with high flow rate, high controllability and low energy consumption.[42]

In this work, Galinstan is used as the core of a liquid metal actuator to induce chaos within the surrounding liquid. The generation of harmonic Marangoni flow is enabled by continuous electrowetting effect at the surface of the liquid metal droplet, upon the application of a sinusoidal AC electric field. The theory behind the operation is developed and validated by conducting experiments with an open-top system. Moreover, a

S.-Y. Tang, Dr. V. Sivan, W. Zhang,
Prof. K. Kanlantar-zadeh, Prof. A. Mitchell,
Dr. K. Khoshmanesh
School of Electrical and Computer Engineering
RMIT University
VIC 3001, Australia
E-mail: shiyang.tang@rmit.edu.au;
kourosh.kalantar@rmit.edu.au; arnan.mitchell@rmit.edu.au;
khashayar.khoshmanesh@rmit.edu.au
P. Petersen
School of Media and Communication
RMIT University
VIC 3001, Australia
P. D. Morrison
School of Applied Sciences
RMIT University
VIC 3001, Australia

DOI: 10.1002/adfm.201400689

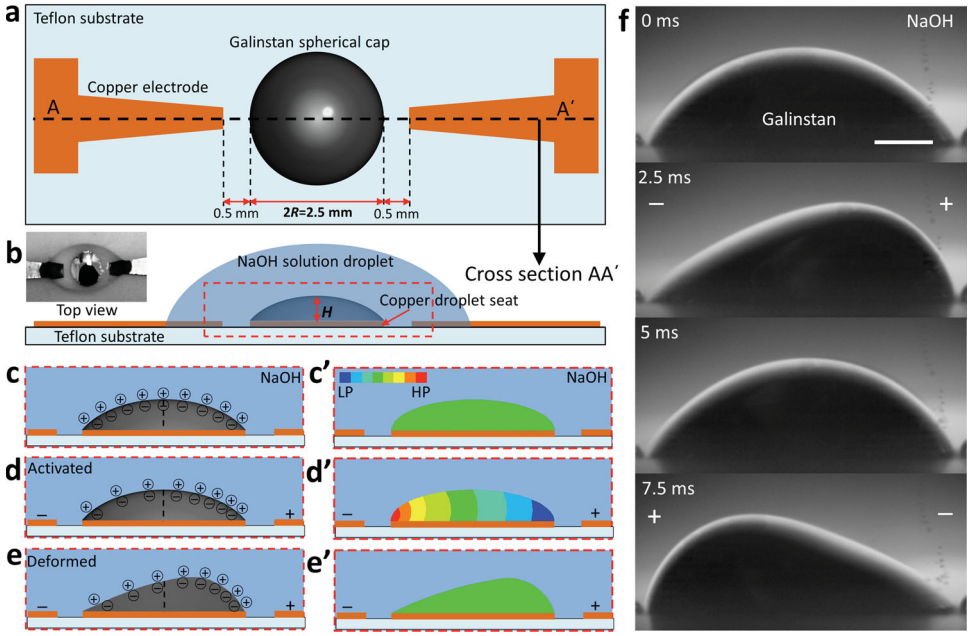

Figure 1. Deformation of the liquid metal actuator. (a) Schematic of the experimental setup, in which a droplet of Galinstan is placed on a circular copper substrate seat with a diameter of 2.5 mm, while the gap between the electrodes is 3.5 mm. (b) Cross-sectional area along the line AA′, a droplet of NaOH solution is placed on a Teflon substrate to cover the Galinstan cap. The inset shows the top view of the system. (c) Charge distribution on the surface of Galinstan cap when immerged in a droplet of NaOH solution, and (c′) Pressure distribution inside the Galinstan cap (LP = low pressure and HP = high pressure). (d) Altered charge distribution on the surface of Galinstan cap immediately after an electric field is applied between the electrodes, and (d′) Altered pressure distribution inside the Galinstan cap. (e) and (e′) Deformation of the Galinstan cap in response to the unbalanced pressure distribution inside the cap. (f) Sequential snapshots of the Galinstan cap when immersed in a NaOH solution (0.3 mol/L), while a sinusoidal wave signal (100 Hz, 4 V) is applied between the two electrodes. Scale bar is 500 μm.

proof-of-concept micromixer is fabricated to demonstrate the viability of the system for microfluidic applications.

2. Results and Discussion

Similar to mercury, Galinstan amalgamates metals such as copper on the surface.[43] In other words, when a droplet of Galinstan is placed on the copper seat, instead of forming a spherical droplet with large contact angle (>90°), the Galinstan droplet is able to spread and wet the surface, forming a spherical cap, as shown in **Figure 1**a and b.

As shown in Figure 1c, when the Galinstan spherical cap is immersed in a droplet of NaOH solution, the surface of the Galinstan is negatively charged, which results in the accumulation of positively charged ions in a diffuse electric double layer (EDL).[39] Surface tension between the liquid metal and the electrolyte depends on the voltage drop across the EDL, as described by Lippman's equation: $\gamma = \gamma_o - \frac{1}{2}cV^2$, where γ is the surface tension, c is the capacitance of EDL per unit area, V is the potential difference across the EDL, and γ_o is the maximum surface tension when $V = 0$.[43] With no external potential, the EDL is initially charged by q_o, which is uniformly distributed along the surface (Figure 1c), inducing a potential difference across the EDL, which can be expressed as: $V_o = q_o/c$.[44]

The pressure difference between the electrolyte and the Galinstan liquid metal p (pressure of Galinstan is higher) at each half of the spherical cap can be obtained from Young-Laplace equation $p = \gamma \frac{4H}{R^2+H^2}$, where H is the height of the spherical cap, and R is radius of the copper seat. Before an external potential is applied, the pressure inside the Galinstan cap is uniform (Figure 1c′). When an external potential is applied, the electrical potential is almost uniform throughout the Galinstan cap due to the high conductivity of the liquid metal. Conversely, the electrolyte has a finite conductivity and thus a potential gradient is generated along the electrolyte. Therefore, as illustrated in Figure 1d, the potential difference across the EDL will be graded from the left side of the Galinstan cap to the right. The voltage drop across the EDL will be lower on the left half of the cap, which results in a higher surface tension, and thus a higher pressure on this half according to Lippman's equation (Figure 1d′). Assuming that the charges in the EDL are uniformly distributed on each half of the Galinstan spherical cap, the surface tension difference $\Delta\gamma$ between the two halves of the spherical cap can be expressed as (detailed in Supporting Information S1):

$$\Delta\gamma = \frac{2R}{L_{gap}} \cdot q_o V_{electrode} \tag{1}$$

where $V_{electrode}$ is the potential applied to the electrodes and L_{gap} is the distance between the electrodes. Accordingly, the pressure difference Δp between the two halves of the spherical cap can be expressed as (detailed in Supporting Information S1):

$$\Delta p = p_L - p_R = \frac{8RH}{L_{gap}\left(R^2 + H^2\right)} \cdot q_o V_{electrode} \tag{2}$$

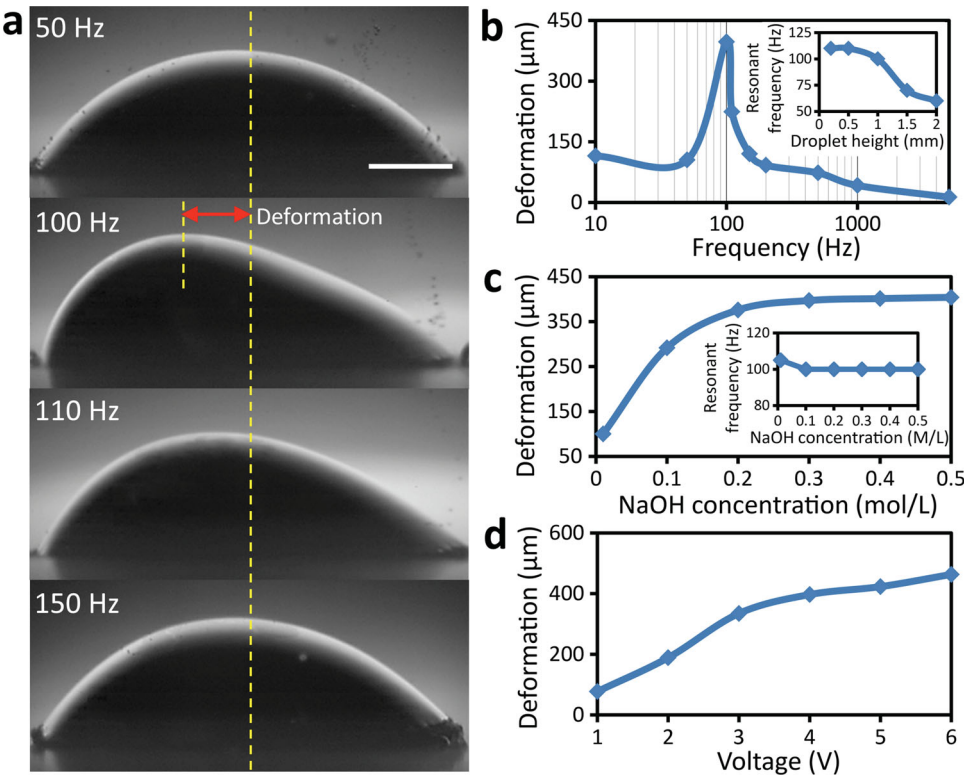

Figure 2. Characterizing the deformation of the Galinstan cap by applying sinusoidal signals with different frequencies and magnitudes, as well as NaOH solutions with different concentrations. Deformation is defined as the distance between the centreline (yellow) and the peak point of the cap. (a) Maximum deformation of Galinstan cap under different frequencies of 50, 100, 110 and 150 Hz (scale bar is 500 μm). (b) Plot for the maximum deformation vs signal frequency in 0.3 mol/L NaOH solution when a 4 V signal is applied, the inset shows variations of the resonant frequency vs cap height *H*. (c) Plot for the maximum deformation vs NaOH concentration when a 100 Hz, 4 V signal is applied, the inset shows variations of the resonant frequency vs NaOH concentration. (d) Plot for the maximum deformation vs magnitude of the signal in a 0.3 mol/L NaOH solution when a 100 Hz signal is applied.

where p_L and p_R are the pressure difference between the Galinstan and the surrounding liquid of the left and the right half of the spherical cap. Since Galinstan liquid metal is non-rigid and the droplet is held still on the copper seat, the imbalance of the pressure inside the Galinstan cap causes its deformation, as shown in Figure 1e. When the deformation reaches its maxima, the pressure distribution within the Galinstan becomes uniform again, leaving the system in equilibrium as shown in Figure 1e′.

A surface tension gradient exists along the interface between the Galinstan cap and the surrounding NaOH as long as the external potential is applied, and the principle for the resulting deformation is called continuous electrowetting (CEW), which is also an electrical analogue to the Marangoni effect.[39,44,45] Figure 1f presents a sequence of high speed images for the continuous oscillating effect of a 3 μL Galinstan spherical cap with a diameter of 2.5 mm and height of ~1 mm, in response to a 100 Hz sinusoidal AC signal with 4 V magnitude. An AC signal is chosen to minimize the electrolysis of the solution. With the application of such a signal, the polarity of the external potential switches periodically, causing the Galinstan cap to oscillate back and forth in response to the applied signal (also shown in Supplementary Movie 1).

The deformation of the Galinstan cap in response to signals of different frequencies ranging from 10 Hz to 10 kHz is investigated. Deformation cannot be observed when the signal frequency is larger than 5 kHz. As an example, **Figure 2**a shows side view images for the maximum deformation of the Galinstan cap during one signal cycle when 50, 100, 110 and 150 Hz signals are applied. The electrical current waveforms are obtained by measuring the voltage across a 1 Ω resistor in series when sinusoidal signals with different frequencies are applied (Supporting Information S2). This indicates that the power consumption for the applied signal with frequencies ranging from 50 to 150 Hz is all about 28 mW. Figure 2b compares the maximum deformation of the Galinstan cap at different frequencies, indicating that the highest deformation occurs at 100 Hz, which we call the mechanical resonant frequency. This mechanical resonant frequency is size dependent. The inset of Figure 2b shows the resonant frequency at different heights (*H*) of Galinstan cap, indicating that the resonant frequency decreases as the size of the Galinstan cap increases.

We also investigate the maximum deformation of the Galinstan cap at different concentrations of the NaOH solution (Figure 2c). The maximum deformation goes up by increasing the ion concentration but becomes saturated at a concentration of 0.3 mol/L. This is because increasing the ion concentration increases the EDL initial charge q_o,[46] and causes a higher pressure difference (Δp) between the two halves of the Galinstan cap, as predicted by Equation (2). However, q_o might become

saturated when the concentration is larger than 0.3 mol/L, beyond which the maximum deformation does not increase. The effect of the ion concentration on the resonant frequency is also studied, as shown in the inset of Figure 2c. It seems that the ion concentration has minimal effect on the Galinstan cap resonant frequency.

The deformation of the Galinstan cap is further investigated by applying signals with different magnitudes. At a constant frequency of 100 Hz, increasing the magnitude of the signal causes more deformation, as shown in Figure 2d. According to Equation (2), increasing the voltage ($V_{electrode}$) intensifies the pressure difference (Δp), which in turn increases the Galinstan cap deformation.

When a sinusoidal signal is applied, the native oxide layer on the surface of Galinstan cap can be electrochemically reduced. Therefore, in order to study the effect of oxide layer formed on the surface of Galinstan on the resonant frequency, we apply a sinusoidal signal of 4 V magnitude with a 4 V DC offset to electrochemically oxidize the anodic pole of the Galinstan cap, as shown in Supporting Information S3. Interestingly, our results show that while the oxide layer formation does reduce the amplitude of oscillation, it has minimal impact on the mechanical resonant frequency, supporting the proposal that this mechanical resonance is determined by the size of the liquid metal.

As long as the external potential is applied, the presence of the surface tension gradient along the interface between the Galinstan cap and the surrounding NaOH produces a tangential force, which pulls the surrounding liquid along the surface from the regions of low surface tension (LST) to the regions of high surface tension (HST), as shown in **Figure 3**a. This motion is known as the Marangoni effect. A series of computational fluid dynamics (CFD) simulations together with high-speed camera imaging measurements are conducted to provide more insight into the observed effect, as detailed in Supporting Information S4. To induce the Marangoni flow presented in Figure 3a, we apply a surface tension gradient along the surface of the Galinstan cap, as given below:

$$\frac{\partial \gamma}{\partial \vec{t}} = \frac{\partial \gamma}{\partial \varphi} \cdot \frac{\partial \varphi}{\partial \vec{t}} = \mu \frac{\partial U}{\partial \vec{n}} \tag{3}$$

where $\vec{t}$ and $\vec{n}$ are the tangential and normal vectors along the surface of Galinstan cap, respectively, μ is the viscosity of the solution surrounding the Galinstan cap, and U is the induced flow velocity at the surface of the Galinstan cap.

Simulations clearly show the induced Marangoni flow along the surface of the Galinstan cap in each half cycle of the sinusoidal AC signal (Figure 3b). The induced flow follows the geometry of the NaOH volume around the Galinstan cap and creates large vortices within in the solution volume, as shown in Figure 3c. The direction of the induced flow changes when the polarity of the applied signal is switched (Figure 3a). Since sinusoidal AC signals are applied, the high surface tension region oscillates back and forth periodically across the metal NaOH interface, dragging the NaOH liquid back and forth. We also add polystyrene particles (diameter of 15 μm) into the NaOH droplet, and record their trajectory by high speed imaging, as shown in Supplementary Movie 2, which clearly shows the fluid actuation is tangential to the metal NaOH interface.

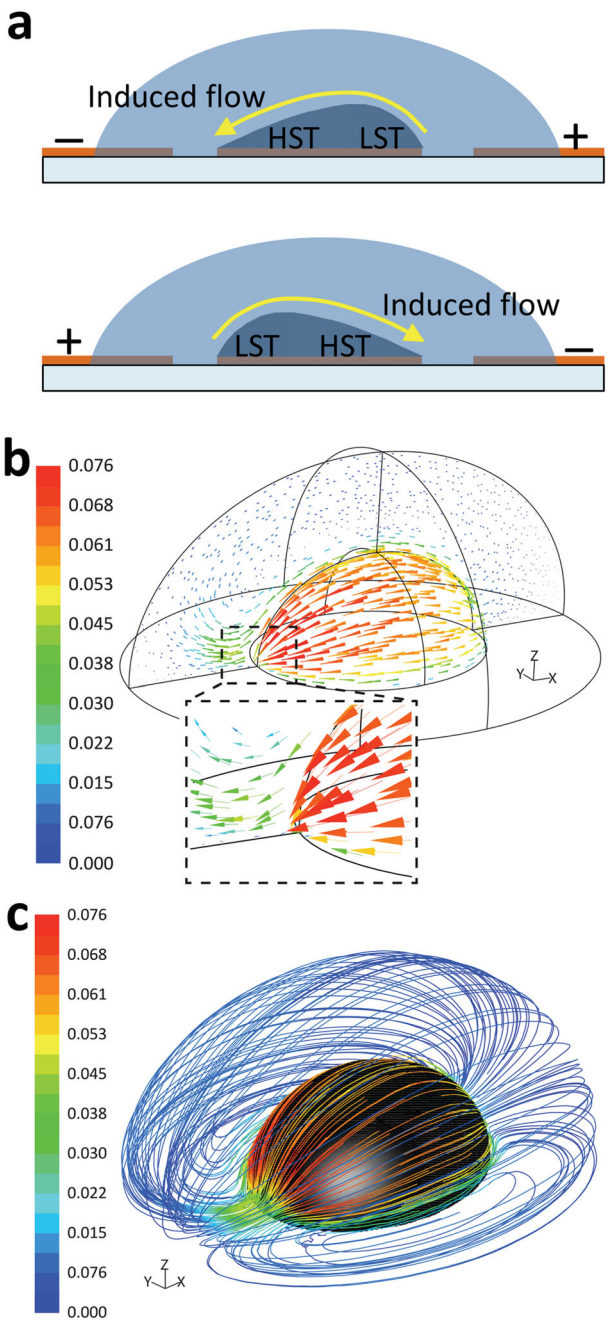

Figure 3. CFD simulations of the liquid metal actuator. (a) Flow velocity vectors (m/s) along the Galinstan surface. (b) Formation of vortices within the surrounding liquid colored by magnitude of flow velocity (m/s).

The generation of vortices due to induced harmonic Marangoni flows is demonstrated using a droplet of NaOH solution with 50 μL volume (with the major and minor radii of ~6 and 9 mm, respectively, and a height of ~3 mm), as shown in the sequential images in **Figure 4**a, when a 4 V, 50 Hz sinusoidal signal is applied. A droplet of dye with 1 μL volume is added to show the trajectory of the vortices (the propagation of the induced Marangoni flow is shown clearly in the high speed movie Supplementary Movie 3). By applying an AC signal,

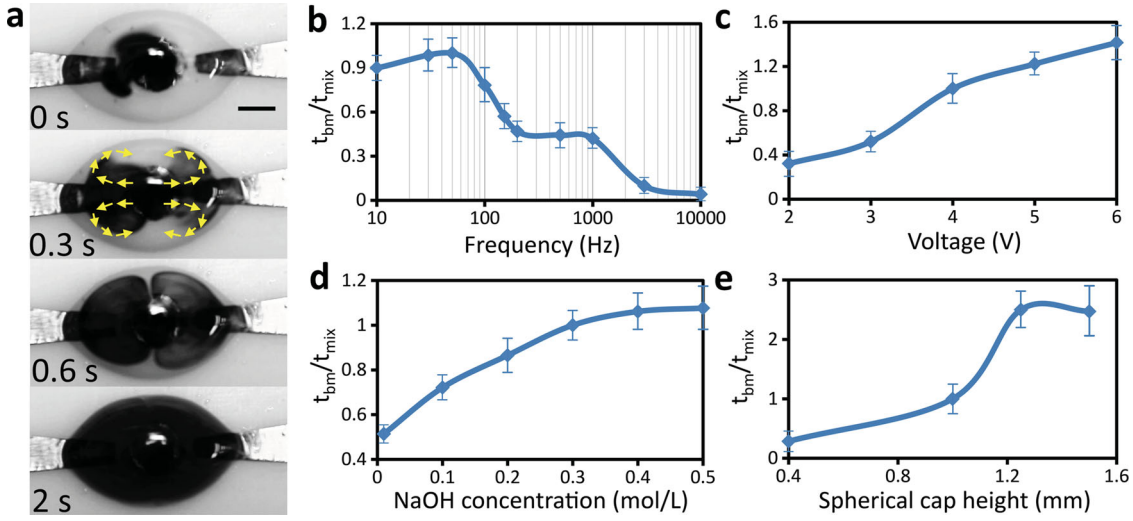

Figure 4. Generation of vortices when a sinusoidal signal is applied. (a) Sequential snapshots for the mixing effect due to generated vortices; a droplet of dye is added to show the trajectory of the vortices. Scale bar is 2 mm. (b) t_{bm}/t_{mix} vs sinusoidal signal frequency plot, obtained with a 50 µL NaOH solution droplet (0.3 mol/L) when 4 V sinusoidal signals of different frequencies are applied. (c) t_{bm}/t_{mix} vs sinusoidal signal magnitude, obtained with a 50 µL NaOH solution droplet (0.3 mol/L) when 50 Hz sinusoidal signals of different magnitudes are applied. (d) t_{bm}/t_{mix} vs NaOH concentration, obtained with a 50 µL NaOH solution droplet when a 50 Hz, 4 V sinusoidal signals is applied. (e) t_{bm}/t_{mix} vs Galinstan cap height H, obtained with a 50 µL NaOH solution droplet (0.3 mol/L) when a 50 Hz, 4 V sinusoidal signal is applied.

large vortices are immediately generated, leading to rapid mixing of the dye with the NaOH solution. The color of the solution becomes homogeneous after ~2.25 s (see Supplementary Movie 4 Part 1). We also examine the consumption of the Galinstan cap by inductively coupled plasma mass spectrometry (ICP-MS) for the working solution. The test is performed under the same conditions described above after 60 s mixing. The results indicate that only gallium can be dissolved into the working solution, with the concentration increasing from 0.15 to 39.62 µmol/L over the duration. Despite this, the liquid metal actuator should be able to operate continuously for at least 8 days before the Galinstan cap loses its eutectic ability (Ga <59.6%)[47] (see Supporting Information S5).

We investigate the mixing performance of the system as a function of frequency and magnitude of the applied AC voltage signal, concentration of the solution, as well as the height of the Galinstan spherical cap. We choose the time required for fully mixing when a 4 V, 50 Hz signal is applied as the bench mark time t_{bm} (~2.25 s). The mixing performance is characterized by obtaining the value of t_{bm}/t_{mix}, where t_{mix} is the actual mixing time for each condition. A larger value of t_{bm}/t_{mix} means a higher mixing rate is achieved. MATLAB software package is used to quantitatively evaluate the performance of mixing by calculating the mass fraction distribution in the NaOH droplet along a multiline path in the captured gray-scale images, and t_{mix} is obtained when the intensity of the color along the paths become saturated. Figure 4b shows the variations of the value of t_{bm}/t_{mix} with respect to different frequencies.

Interestingly, although the observed deformation of the Glainstan cap reaches its maximum at 100 Hz, our observations show that the highest mixing rate is achieved when the frequency of the signal is set to 50 Hz, in which the observed deformation of the Galinstan cap is small (Figure 2). This further confirms that the mixing effect is not due to the mechanical deformation of the Galinstan cap as the best mixing should happen with the maximum displacement. We conduct a series of control experiments to further explore the mechanism of the mixing effect. Firstly, in the absence of the Galinstan spherical cap, no mixing effect is observed, ruling out electro-osmosis as the driving mechanism of the induced flow (see Supporting Information S6). Secondly, experiments using a solid solder alloy ($Sn_{50}Zn_{49}Cu_1$) spherical cap with a thin layer of Galinstan coating lead to a high mixing rate similar to that of Galilnstan liquid metal without moving the cap, confirming that the mixing effect is attributed to the Marangoni flow of the fluid tangential to the surface, and not the displacement of fluid due to the mechanical deformation of the Galinstan cap (see Supporting Information S6).

At a constant frequency of 50 Hz, the mixing performance is characterized by applying signals with different magnitudes. Increasing the magnitude of the signal enhances the mixing, as shown in Figure 4c. According to Equation (1), increasing the voltage ($V_{electrode}$) tends to intensify the surface tension difference ($\Delta\gamma$), which in turn provides a stronger mixing. However, undesired bubble generation due to the electrolysis occurs on the electrodes when the magnitude of the applied signal is larger than 6 V at 100 Hz.

The mixing performance is further investigated by changing the ion concentration of the solution (Figure 4d). Increasing the ion concentration causes the increase of the EDL initial charge q_o,[46] leading to a higher surface tension difference, as predicted by Equation (1). However, q_o might become saturated when the concentration is larger than 0.3 mol/L, beyond which the mixing rate is saturated.

Our observations show that increasing the cap height also enhances the mixing performance (Figure 4e). This can be attributed to the fact that enlarging the surface of the Galinstan cap leads to faster agitation of the surrounding NaOH solution.

The mixing performance in response to different NaOH solution volumes is also studied. Results indicate that increasing the volume of the solution increases the time required to achieve full mixing (see Supporting Information S7). Furthermore, the performance of the system for mixing of liquids with various viscosities is investigated by adding glycerol to DI water. The results show that our system is able to mix a liquid, which is up to ~100 times more viscous than DI water (see Supporting Information S7). The system is also capable of mixing other solutions including NaCl and PBS, as shown in part 2 and 3 of Supplementary Movie 4.

However, the system does not operate with acidic electrolytes of pH less than 6.5, which could potentially be attributed to the formation of a solid oxide layer on the surface of Galinstan cap at such a low pH. In order to test this, we conduct experiments using a ~0.8 pH electrolyte containing 6% HCl to assure that this oxide layer is removed.[48] However, even in this case, mixing of the surrounding liquid cannot be observed, indicating that the inhibition of mixing at low pH solutions is not due to the formation of solid oxide layer. We believe another potential explanation could be that the formation of gallates ($[Ga(OH)_4]^-$) on the surface of Galinstan liquid metal in a basic solution is essential to create a large potential drop across the electrical double layer.[39,42] However, no such gallate can be formed in an acidic environment, thus the surface tension modification of Galinstan that would occur by dropping potential across the electrical double layer can hardly occur in an acidic environment.[39] As such, no Marangoni flow can be generated in acidic solution and hence no mixing occurs.

The capability of the system is further demonstrated by mixing a droplet of oil with the NaOH solution. We add a 5 µL sunflower oil droplet into the NaOH solution and apply a 50 Hz, 4 V sinusoidal signal to activate the electrodes. **Figure 5**a shows the NaOH-oil suspension 2 and 14 s after activating the electrodes (also shown in Supplementary Movie 5). In order to obtain the size of the oil droplets following the mixing, we immediately transfer the agitated NaOH-oil suspension onto a glass substrate with a length scale etched on its surface. We use an inverted microscope to take images and analyse them using the Nikon NIS-Elements software, as shown in Figure 5b. The generated vortices are capable of mixing the oil droplet efficiently with the NaOH solution, and the size of the oil droplets becomes smaller by prolonging the mixing time (see Figure 5b inset).

We further examine the application of our actuator as a micromixer by integrating it into a microfluidic system. We place a polydimethylsiloxane (PDMS) microchannel with dimensions of 600 × 150 µm (W×H) with two parallel inlets onto a polymethyl methacrylate (PMMA) substrate, which has a cylindrical Galinstan cap seat with a diameter of 3 mm and depth of 500 µm to hold the Galinstan cap (**Figure 6**a). A Galinstan cap with a diameter of 2.5 mm and height of 400 µm is placed in the cylindrical seat and activated by two copper electrodes (see Supporting Information S8 for detailed design). During the experiment, uncolored NaOH solution with the concentration of 0.01 mol/L is added into Inlet-1 while blue NaOH solution (with added blue dye) with the same concentration is added into Inlet-2. We investigate the capability of the system for mixing the flows coming from Inlets 1 and 2 at various flow rates, ranging from 25 to 100 µL/min (see Supplementary Movie 6).

As an example, Figure 6b shows the microchannel when the flow rate is set to 75 µL/min before the mixer is activated. The flow is purely laminar due to its low Reynolds number (Re < 5) and the mixing only happens at the interface of incoming flows, as evidenced by formation of a clear boundary between the colored and uncolored solutions along the middle of the microchannel. When a 50 Hz, 4 V sinusoidal signal is applied, a strong instability is induced in the liquid surrounding the Galinstan cap due to creation of induced harmonic Marangoni flows. This instability mixes the incoming flows, and meanwhile propagates along the channel by following the direction of the flow (Figure 6c), providing a high mixing efficiency even

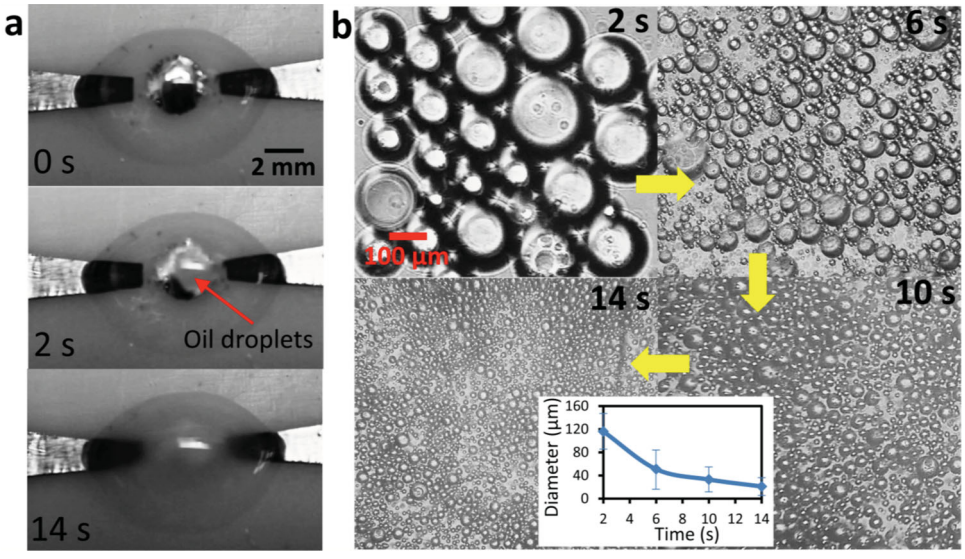

Figure 5. Application of the system for mixing NaOH solution with oil droplets. (a) Sequential snapshots for the mixing between the NaOH solution and a droplet of oil. (b) Shrinkage of oil droplets in the NaOH-oil suspension after 2, 6, 10 and 14 s mixing, respectively. The inset shows the variations of diameter vs time plot for the oil droplets.

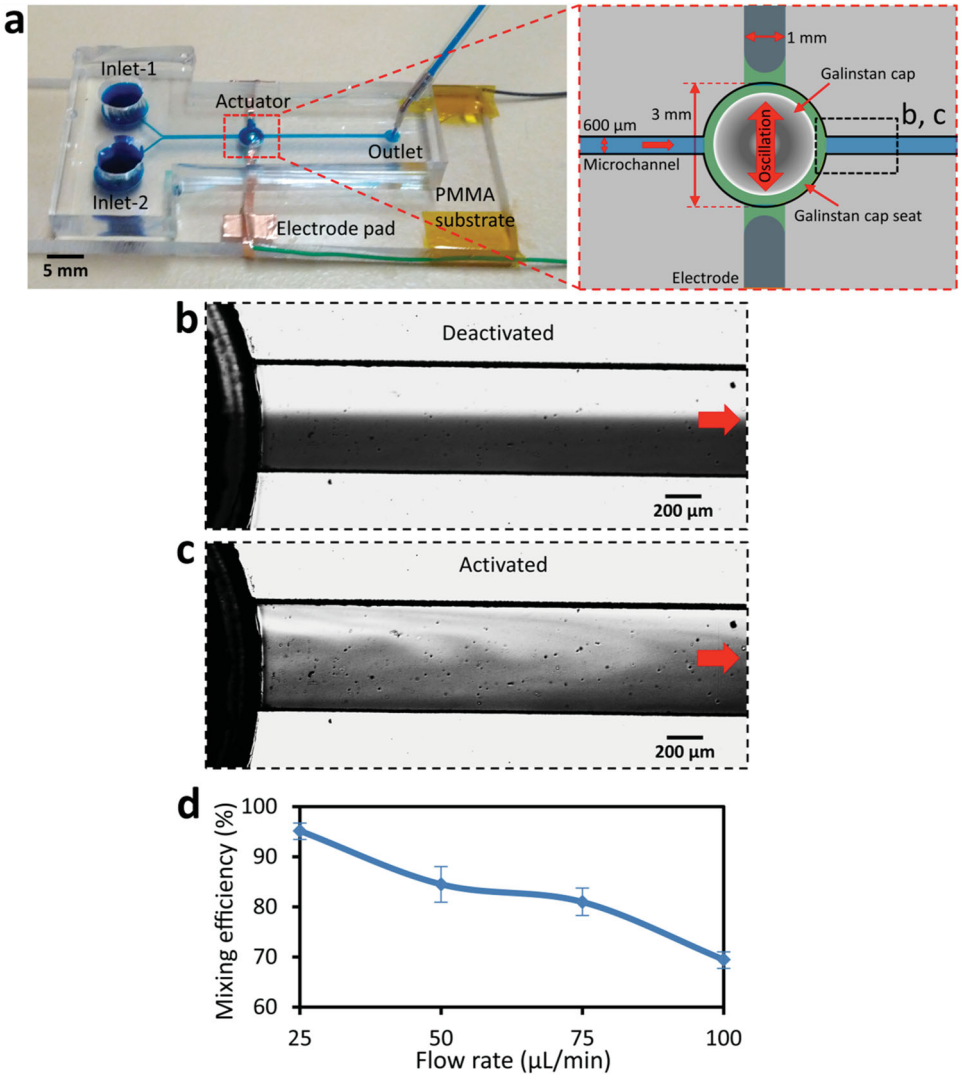

Figure 6. Experiments with the microfluidic system. (a) The overall microfluidic system using a PDMS microchannel with two parallel inlets assembled onto a PMMA platform. The wires are bonded to the electrode pads by copper tapes. The subset shows the detailed actuator part. (b) Distribution of neighboring flows in the microchannel before the mixer is activated when the flow rate is set to 75 µL/min. (c) Distribution of neighboring flows after the mixer is activated. (d) Mixing efficiency vs flow rate plot, obtained when a 50 Hz, 4 V sinusoidal signal is applied.

at high flow rates (also shown in Supplementary Movie 6). The mixing efficiency of the system is evaluated by calculating the mass fraction distribution at 2 mm downstream of the Galinstan cap using the described image analysis MATLAB code (see Supporting Information S9 for details). The time averaged mixing efficiency is calculated as 95, 84, 80 and 70% at the flow rates of 25, 50, 75 and 100 µL/min, respectively (Figure 6d). The power consumption based on the obtained voltage and current waveforms is calculated as 0.3 mW. The described micromixer has no mechanical parts and can be easily fabricated and implemented into a lab-on-a-chip platform.

3. Conclusion

We have validated the theory behind the operation, and demonstrated the capabilities of our liquid metal actuator for inducing chaotic advection, based on continuous electrowetting effect. Induced harmonic Marangoni flows can be induced by applying a sinusoidal signal, generating vortices in the solution. More importantly, such an actuator has been integrated into a microfluidic system, achieving high mixing efficiencies even at high flow rates. This liquid metal actuator offers unique advantages including simple fabrication, low-cost, low operating voltage, low power consumption, as well as high controllability. However, it should be considered that the actuator can only operate in basic solution and also gradually leaches out low concentrations of gallium ions into the solution. Further research is required to gain improved understanding of the electrochemistry of this structure which may suggest approaches to minimise these negative effects. Such liquid metal actuator has the potential to enable highly complex, yet practical applications in the areas of micro-cooling, MEMS actuation and microfluidics, to realize dynamically reconfigurable electro-mechanical systems.

4. Experimental Section

Experiment Setup: A copper tape with a diameter and thickness of 2.5 mm and 35 μm, respectively, is sticked to a Teflon substrate to serve as droplet seat and a Galinstan (68.5% gallium, 21.5% indium and 10% tin) droplet is placed onto it. The electric field is imposed by a signal generator (Tabor, 2572A 100 MHz Dual-Channel) between the two strips of copper tapes, located on both sides of the seat, which serve as electrodes (Figure 1a and b). The Galinstan droplet and the tips of the electrodes are immersed in a droplet of NaOH solution. Teflon substrate is chosen due to its hydrophobic surface, enabling the NaOH solution to cover the Galinstan cap instead of spreading on the surface of the substrate. Teflon substrate also facilitates the removal of liquid droplet during experiment process. Experiments are repeated three times and the data presented as mean ± standard error. For experiments using microfluidic platform, polydimethylsiloxane (PDMS) microchannels are fabricated using standard photolithography techniques.[49]

High Speed Camera Imaging: The vibration of the Galinstan cap and the trajectories of the surrounding liquid are captured using a high-speed camera (PHANTOM MIRO M-310, Vision Research Inc.) fitted with a MACRO-NIKKOR 65 mm lens, PB-6 belows and PK-11 extension tube. Tungsten light heads (Dedocool Lights) are used for illumination.

Mixing Performance Analysis: The image processing toolbox of MATLAB software package (MathWorks, 2010a) is used to assess the mixing efficiency of the system. An inverted microscope (Nikon Eclipse, TE 2000) is used to obverse the performance of the system in some experiments.

Supporting Information

Supporting Information is available from the Wiley Online Library or from the author.

Acknowledgements

K. Khoshmanesh acknowledges the Australian Research Council for funding under Discovery Early Career Researcher Award (DECRA) scheme, (project DE120101402).

Received: February 28, 2014
Revised: May 23, 2014
Published online: July 14, 2014

[1] M. Chertkov, V. Lebedev, *Phys. Rev. Lett.* **2003**, *90*, 134501.
[2] A. Priye, Y. A. Hassan, V. M. Ugaz, *Anal. Chem.* **2013**, *85*, 10536–10541.
[3] A. Tohidi, S. M. Hosseinalipour, P. Taheri, N. M. Nouri, A. S. Mujumdar, *Heat Mass Transfer* **2013**, *49*, 1535–1548.
[4] A. Lefèvre, J. P. B. Mota, A. J. S. Rodrigo, E. Saatdjian, *Int. J. Heat Fluid Flow* **2003**, *24*, 310–321.
[5] G. Metcalfe, D. Lester, A. Ord, P. Kulkarni, M. Trefry, B. E. Hobbs, K. Regenaur-Lieb, J. Morris, *Philos. Trans. R. Soc., A* **2010**, *368*, 217–230.
[6] P. Sundararajan, A. D. Stroock, *Chem. Biomol. Eng.* **2012**, *3*, 473–496.
[7] A. D. Stroock, S. K. Dertinger, A. Ajdari, I. Mezić, H. A. Stone, G. M. Whitesides, *Science* **2002**, *295*, 647–651.
[8] D. Therriault, S. R. White, J. A. Lewis, *Nat. Mater.* **2003**, *2*, 265–271.
[9] T. H. Solomon, I. Mezić, *Nature* **2003**, *425*, 376–380.
[10] R.-T. Tsai, C.-Y. Wu, *Biomicrofluidics* **2011**, *5*, 014103.
[11] D. S. Kim, S. W. Lee, T. H. Kwon, S. S. Lee, *J. Micromech. Microeng.* **2004**, *14*, 798.
[12] H. Xia, S. Wan, C. Shu, Y. Chew, *Lab Chip* **2005**, *5*, 748–755.
[13] Z. Chen, M. Bown, B. O'Sullivan, J. MacInnes, R. Allen, M. Mulder, M. Blom, R. van't Oever, *Microfluid. Nanofluid.* **2009**, *6*, 763–774.
[14] J. Cha, J. Kim, S.-K. Ryu, J. Park, Y. Jeong, S. Park, S. Park, H. C. Kim, K. Chun, *J. Micromech. Microeng.* **2006**, *16*, 1778.
[15] Y. K. Suh, S. Kang, *Micromachines* **2010**, *1*, 82–111.
[16] T. Frommelt, M. Kostur, M. Wenzel-Schäfer, P. Talkner, P. Hänggi, A. Wixforth, *Phys. Rev. Lett.* **2008**, *100*, 034502.
[17] T.-D. Luong, N.-T. Nguyen, *Micro Nanosyst.* **2010**, *2*, 217–225.
[18] R. J. Shilton, L. Y. Yeo, J. R. Friend, *Sens. Actuat. B* **2011**, *160*, 1565–1572.
[19] B. Xu, T. N. Wong, N.-T. Nguyen, Z. Che, J. C. K. Chai, *Biomicrofluidics* **2010**, *4*, 044102.
[20] B. Xu, T. N. Wong, N.-T. Nguyen, *Heat Mass Transfer* **2011**, *47*, 1331–1339.
[21] R. O. Grigoriev, M. F. Schatz, V. Sharma, *Lab Chip* **2006**, *6*, 1369–1372.
[22] J. Deval, P. Tabeling, C.-M. Ho, at Micro Electro Mechanical Systems, 2002. The Fifteenth IEEE International Conference on, IEEE: **2002**, 36–39.
[23] S. Qian, H. H. Bau, *Anal. Chem.* **2002**, *74*, 3616–3625.
[24] M. Oddy, J. Santiago, J. Mikkelsen, *Anal. Chem.* **2001**, *73*, 5822–5832.
[25] J. D. Posner, C. L. Pérez, J. G. Santiago, *Proc. Natl. Acad. Sci. USA* **2012**, *109*, 14353–14356.
[26] A. O. El Moctar, N. Aubry, J. Batton, *Lab Chip* **2003**, *3*, 273–280.
[27] J.-H. So, M. D. Dickey, *Lab Chip* **2011**, *11*, 905–911.
[28] P. Paik, V. K. Pamula, M. G. Pollack, R. B. Fair, *Lab Chip* **2003**, *3*, 28–33.
[29] C.-C. Chang, R.-J. Yang, *Microfluid. Nanofluid.* **2007**, *3*, 501–525.
[30] H.-J. Koo, J.-H. So, M. D. Dickey, O. D. Velev, *Adv. Mater.* **2011**, *23*, 3559–3564.
[31] T. Liu, P. Sen, C.-J. Kim, *J. Microelectromech. Syst.* **2012**, *21*, 443–450.
[32] M. D. Dickey, R. C. Chiechi, R. J. Larsen, E. A. Weiss, D. A. Weitz, G. M. Whitesides, *Adv. Funct. Mater.* **2008**, *18*, 1097–1104.
[33] C. Ladd, J.-H. So, J. Muth, M. D. Dickey, *Adv. Mater.* **2013**, *25*, 5081–5085.
[34] S. Zhu, J.-H. So, R. Mays, S. Desai, W. R. Barnes, B. Pourdeyhimi, M. D. Dickey, *Adv. Funct. Mater.* **2013**, *23*, 2308–2314.
[35] J. Park, S. Wang, M. Li, C. Ahn, J. K. Hyun, D. S. Kim, J. A. Rogers, Y. Huang, S. Jeon, *Nat. Commun.* **2012**, *3*, 916.
[36] D. J. Lipomi, B. C. K. Tee, M. Vosgueritchian, Z. Bao, *Adv. Mater.* **2011**, *23*, 1771–1775.
[37] T. Krupenkin, J. A. Taylor, *Nat. Commun.* **2011**, *2*, 448.
[38] V. Sivan, S.-Y. Tang, A. P. O'Mullane, P. Petersen, N. Eshtiaghi, K. Kalantar-zadeh, A. Mitchell, *Adv. Funct. Mater.* **2013**, *23*, 144–152.
[39] S.-Y. Tang, V. Sivan, K. Khoshmanesh, A. P. O'Mullane, X. Tang, B. Gol, N. Eshtiaghi, F. Lieder, P. Petersen, A. Mitchell, K. Kalantar-zadeh, *Nanoscale* **2013**, *5*, 5949–5957.
[40] X. Tang, S.-Y. Tang, V. Sivan, W. Zhang, A. Mitchell, K. Kalantar-zadeh, K. Khoshmanesh, *Appl. Phys. Lett.* **2013**, *103*, 174104.
[41] W. Zhang, J. Z. Ou, S.-Y. Tang, V. Sivan, D. D. Yao, K. Latham, K. Khoshmanesh, A. Mitchell, A. P. O'Mullane, K. Kalantar-zadeh, *Adv. Funct. Mater.* **2014**, *24*, 3799–3807.
[42] S.-Y. Tang, K. Khoshmanesh, V. Sivan, P. Petersen, A. P. O'Mullane, D. Abbott, A. Mitchell, K. Kalantar-zadeh, *Proc. Natl. Acad. Sci. USA* **2013**, *111*, 3304–3309.
[43] P. Huttenloch, K. E. Roehl, K. Czurda, *Environ. Sci. Technol.* **2003**, *37*, 4269–4273.
[44] G. Beni, S. Hackwood, J. Jackel, *Appl. Phys. Lett.* **1982**, *40*, 912–914.
[45] H. J. Lee, C.-J. Kim, *J. Microelectromech. Syst.* **2000**, *9*, 171–180.
[46] D. C. Grahame, *Chem. Rev.* **1947**, *41*, 441–501.
[47] G. N. van Ingen, J. Kapteijn, J. L. Meijering, *Scripta Metallurgica* **1970**, *4*, 733–736.
[48] V. Kocourek, C. Karcher, M. Conrath, D. Schulze, *Phys. Rev. E: Stat., Nonlinear, Soft. Matter Phys.* **2006**, *74*, 026303.
[49] K. Kalantar-Zadeh, B. N. Fry, *Nanotechnology-enabled Sensors*, Springer, New York, US **2008**.